Event-Locked Time-Resolved Fourier Spectroscopy

H. WEIDNER and R. E. PEALE*

Department of Physics, University of Central Florida, Orlando, Florida 32816

A low-cost method of adding time-resolving capability to commercial Fourier transform spectrometers with a continuously scanning Michelson interferometer has been developed. This method is specifically designed to eliminate noise and artifacts caused by mirror-speed variations in the interferometer. The method exists of two parts: (1) a novel timing scheme for synchronizing the transient events under study and the digitizing of the interferogram and (2) a mathematical algorithm for extracting the spectral information from the recorded data. The novel timing scheme is a modification of the well-known interleaved, or stroboscopic, method. It achieves the same timing accuracy, signal-to-noise ratio, and freedom from artifacts as step-scan time-resolving Fourier spectrometers by locking the sampling of the interferogram to a stable time base rather than to the occurrences of the HeNe fringes. The necessary pathlength-difference information at which samples are taken is obtained from a record of the mirror speed. The resulting interferograms with uneven pathlength-difference spacings are transformed into wavenumber space by least-squares fits of periodic functions. Spectra from the far-infrared to the upper visible at resolutions up to 0.2 cm^{-1} are used to demonstrate the utility of this method.

Index Headings: Spectroscopy; Fourier; Time-resolved.

INTRODUCTION

Time-resolved Fourier transform spectroscopy (TRFTS) is a powerful tool in a variety of applications. TRFTS adds time resolution to the proven advantages of Fourier transform spectroscopy (FTS), namely, the combination of wide-spectral coverage, high resolution, and good signal-to-noise ratios. Among the problems studied so far are kinetics of chemical reactions,[1] liquid–crystal reorientation dynamics,[2] photoluminescence of porous silicon,[3] and energy-transfer processes in activated optical materials.[4] The number and diversity of applications can be expected to increase as the technique comes into wider use. At the time of this writing, only step-scan interferometers commercially offer high-performance time-resolving capabilities over a wide range of time constants. These machines are substantially more expensive than continuous-scan machines, which have a relatively simple drive mechanism. Since the number of existing continuous-scan instruments in the field is very large, there is reason to seek a TRFTS method that can work with any continuous-scan machine without significant changes in its existing hardware. The most general implementation of TRFTS on continuously scanning instruments involves stroboscopic or interleaved data acquisition. Though a significant increase in signal-to-noise ratio and a reduction in artifacts is achieved by using a reference channel,[5] the interleaved method still suffers from the timing jitter introduced by variations in the speed of the traveling mirror.[4]

We developed a new method of time-resolved spec-

troscopy with continuously scanning interferometers that improves the timing accuracy to the level of step-scan systems and that also allows the use of a reference detector. It does not require changes to the interferometer hardware besides the optional addition of an optical retarder plate[4,6] and can be added to any continuously scanning interferometer. A first implementation with 1 μs resolution is presented here. It uses standard electronics to keep the cost low, a novel timing scheme for data acquisition, and a novel algorithm to obtain the spectra.

EXPERIMENTAL

Fundamentals. The usual principles of FTS are illustrated in Fig.1. Light emitted from (or passed through) a sample is modulated by a Michelson interferometer as a function of pathlength difference. The modulated intensity is digitized at evenly spaced moving-mirror positions and collected as an interferogram. The spacing between the sampling locations is often determined by the interference pattern of a red HeNe laser that shares the same interferometer optics as the signal of interest. According to Nyquist's sampling theorem, frequencies up to 7899 cm^{-1} can be characterized with one sample per laser fringe. Higher optical frequencies require more samples per fringe. Spectral resolution is determined by the length of the moving-mirror scan, i.e., the maximum pathlength difference. The interferogram contains the complete spectral information. Therefore, the task of *time-resolved* Fourier spectroscopy is the acquisition of all interferogram points at the desired observation times during a transient event. With the exception of very slow transients, it is impossible to obtain the necessary data from a single transient. One alternative is to create one transient per data point. Step-scan interferometers set their mirrors to each pathlength difference to be sampled, and (at least) one transient is initiated and recorded at each of these positions.

In contrast, continuously scanning interferometers take data "on the fly". The temporal HeNe interference pattern triggers a continuous stream of requests to sample the interferogram, ensuring even sample spacing. The transient signal needs to be prepared with the proper time delay at the time of each sampling request. A number of TRFTS schemes have been developed to deal with the continuous stream of sampling requests issued by continuously scanning interferometers. For transients that are short and have a creation rate that can equal the sampling rate, a transient can be initiated at each sample request, and the actual sampling occurs after the desired delay time.[1] For even higher repetition rates, asynchronous TRFTS is possible.[7] If the transients last longer than the time between sampling requests (even at slow mirror speeds) and/or they cannot be repeated at a high enough rate, one has to use the interleaved scheme[1,4,8] where sam-
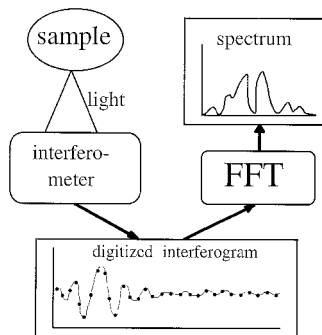
FIG. 1. Illustration of the principle of Fourier spectroscopy. The interferometer modulates the light. The digitized interferogram is analyzed by using fast Fourier transform (FFT) to obtain the spectrum.

FIG. 2. Timing diagram for traditional interleaved TRFTS. The sampling of the interferogram is locked to the HeNe reference, assuring accurate knowledge of the sampling positions, which are evenly dispersed in space. However, mirror-speed variations cause interferogram points to be recorded at uneven time intervals.

ple requests are skipped and multiple mirror sweeps are used to collect a single complete interferogram for a particular time delay. A key feature of this scheme, which also limits performance, is the rigid locking of the interferogram sampling to the HeNe reference. This rigid locking not only limits the timing accuracy and hence the time resolution but is also a significant source of noise.[4]

Figure 2 shows a timing diagram for traditional interleaved TRFTS. Transient events are triggered in fixed relation to the HeNe reference. The variable delay is chosen (and then kept fixed) to initiate an event at a desired time before a series of analog-to-digital converter (ADC) samples, which are also locked to the HeNe reference (dashed lines). Mirror-speed variations make the prediction of the arrival times of the reference pulses uncertain, which results in a timing jitter with respect to the event initiation. This timing jitter causes an uncertainty in the spectral content of the transient at the actual time of sampling. It can also cause uncertainty in the total (modulated plus unmodulated) signal seen by the detector. If the total signal at the expected sample time is changing at a rate dI/dt, a timing error of Δt translates into an intensity error of $\Delta I = \Delta t \, dI/dt$, which appears as noise in the interferogram. This causes noisy spectra and, if the mirror-speed variations are not entirely random, artifacts. The solution would seem to be perfect stabilization of the mirror speed. Sophisticated systems like the Bomem DA8 achieve stability at up to 2% of the intended speed.[4] However, further stabilization, even by only a small factor, is likely accompanied by large expenses, more or less permanent changes to the hardware, and a reduction in flexibility for varied spectroscopic applications. Timing jitter from mirror-speed variations, therefore, will remain a significant source of noise and artifacts for realistic continuous-scan TRFTS systems based on traditional methods.

Event-locked TRFTS. Our solution to the problem of timing jitter from mirror-speed variations is to decouple the ADC samples from the temporal HeNe fringe pattern. Instead, we sample the transient signal exactly at the times of interest, independently of the exact mirror position. The (unevenly spaced) pathlength differences at which the samples were taken are established by measuring the speed of the mirror during the sampling. Since sampling of the interferogram and the speed recording are now locked to the transient event rather than to the HeNe reference, the name "*event*-locked TRFTS" was chosen.
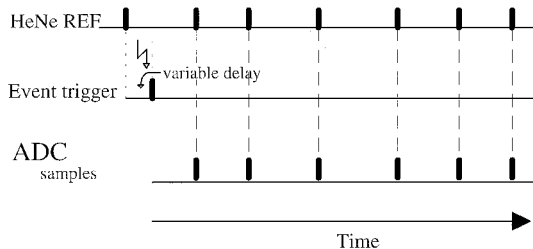
Figure 3 shows how the data-acquisition processes are locked to a synchronizing event (SYNC). We suppose that the transients are excited by a Q-switched laser as a concrete example of general interest. The SYNC signal starts the recording of the speed information (see "implementation" for details) and two counters, which control the pulsed laser and the ADC. Both counters have a programmable delay and a programmable pulse width. The beginning of the laser-control pulse may be used to prepare each transient, and its end initiates the transient. In our setup, these are the firing of the laser flash lamps and the actual laser shot by triggering the Q-switch, respectively. The ADC control counter sets the length of the sampling window and its relative position to the initiation of the transient. The ADC is paced by a quartz-stabilized time base at a rate that is independent of the HeNe laser-fringe frequency. It can be very useful to position part of the sampling window before the initiation of the transient, as is shown in Fig. 3. Zero signal levels or spectral information immediately before the transient can be recorded during this time.

The SYNC signal can be derived from practically any source (for instance a ready signal from a free-running laser). It is, however, necessary to know the number of the HeNe reference pulse (REF) just before SYNC to determine the pathlength-difference information from the recorded speed and the times of the ADC samples. If the
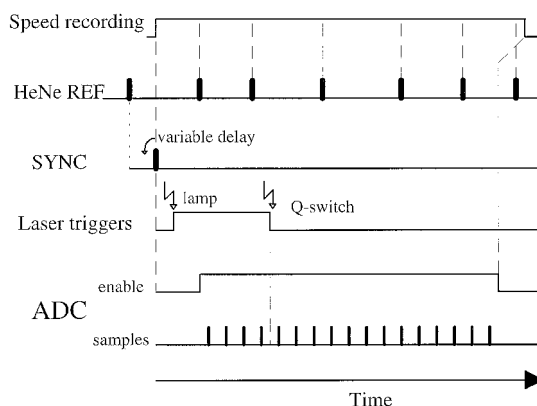
FIG. 3. Timing diagram for event-locked TRFTS. The acquisition of interferogram information is locked to a SYNC event and decoupled from the HeNe laser fringe pattern. Connection to the pathlength difference is established numerically from a record of the arrival times of HeNe reference pulses measured during the sampling period of the ADC. Triggering of a Q-switched laser is indicated as an example of an excitation scheme for transient events.

Intensity

pathlength difference
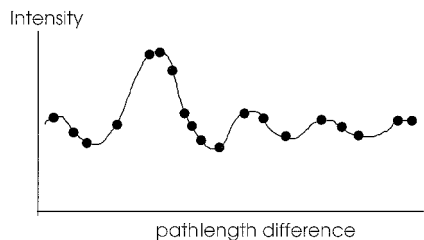
FIG. 4. Interferogram with uneven sample spacing, as would be obtained with large variations of the mirror speed for sampling at constant time intervals.

excitation source is triggerable, a REF pulse can be used as the SYNC signal as shown in Fig. 3. By selecting an appropriate sequence of REF pulses, one can spread the transient events and, thus, the acquired samples almost evenly over the length of the mirror scan. A free-running laser would require a considerably larger number of transient events to assure measurements near all necessary pathlength differences. An additional delay between the counter-selected REF pulse and the SYNC pulse allows an even finer spread of events. The delay may be varied over a number of mirror sweeps to obtain a sequence of measurements with transient events slightly shifted with respect to the HeNe fringe pattern, thus acquiring several samples per HeNe fringe. Such sampling is necessary for near-infrared (IR), visible, and ultraviolet (UV) measurements. The number of different time delays can be chosen so that the Nyquist critical frequency exceeds the maximum frequency present in the interferogram. Since there is no restriction of this number, for instance, to integer powers of 2 the number of samples and transient events may be kept minimal. The delay is realized by a digital counter that causes discreteness of the actual delay times and may prevent division of the HeNe fringes into exactly equal intervals. However, this is not a problem since the exact pathlength difference of all samples is determined. A potential loss of spectral information caused by an unequal division can be avoided by using a sufficiently large number of different delays.

The recorded speed information is a list of time differences $\{\tau_i\}$ for $i = 0 \ldots n - 1$, where τ_0 is the time between the SYNC pulse and the first REF pulse, and subsequent τ_i are the times between the ith and $(i + 1)$th REF pulses. The routine "spline" from Ref. 9 has been modified to accept the data as recorded and to utilize the fact that the dependent variable is the fringe number i. The cubic-spline interpolation done by this routine delivers a continuous function representing fringe number vs. time. This function is evaluated at the time delay of an ADC sample and gives the pathlength advancement since the last REF pulse before SYNC. The actual pathlength difference is found by adding the (integer) fringe number of the last REF pulse before SYNC. This procedure is repeated for all interferogram points for the desired time delay. The result is a list of interferogram intensities, y_i, with their respective pathlength differences, x_i. A hypothetical plot of such an interferogram is shown in Fig. 4, where the uneven spacing between points has been exaggerated.

Obtaining the Spectra. The analysis of unevenly spaced interferogram data cannot, in general, directly rely on the usual fast Fourier transform to convert interferogram information into spectral information (spectral density and phase). The FFT is based on the assumption of even data point spacing. In other words, FFT weights the data on a "per interval" basis. In contrast, least-squares (LS) fitting weights the data on a "per point" basis[9] and can handle unequal spacing. Here, we describe the concepts of the analysis process. A derivation of the equations involved is given in the Appendix.

There are two main analysis steps: (1) determination of the complex spectral density and (2) estimation and removal of unwanted phase information. Both steps rely on LS fits of harmonic functions (Eq. 1) to the interferogram data. The phase offset, ϕ, arises from frequency-dependent differences in optical pathlength caused mainly by asymmetries in the beamsplitter. Therefore, ϕ varies only slowly with σ, and a low-resolution double-sided interferogram is often sufficient to characterize the phase function, $\phi(\sigma)$.[10] Such an interferogram can be obtained by beginning the data acquisition a distance x_z (~ 1 mm) before $x = 0$ and using only data in the range $[-x_z, x_z]$ to determine ϕ as outlined in the Appendix. The phase function can now be considered as known, and thus the amplitude, A, of the harmonic functions is the only fitting parameter for the higher resolution interferogram. Evaluating A for the frequencies of interest gives the phase-corrected spectrum.

Our LS method is equivalent to established methods of spectral analysis in the case of equally spaced interferogram points. Furthermore, the similarities between LS fitting and FFT calculation point the way for implementation of apodizations[10] and other procedures proven useful for the analysis of interferograms.

The evaluation described in the Appendix has relatively large memory requirements (32 megabytes for spectra up to 22,000 cm^{-1} at 0.1 cm^{-1} resolution). Without data reduction, conventional FFT based on equally spaced interferograms requires only one eighth of the memory and is approximately 16 times faster. However, computers with sufficient memory and speed to make these considerations a trivial concern are now widely available at low cost.

Implementation. We have implemented the hardware and software for the acquisition and the analysis of time-resolved spectral information using the event-locked technique. Our goal was a low-cost system with a time resolution of 1 μs. An overview of the setup is shown in Fig. 5. We use a DA8 spectrometer from Bomem, but our implementation could easily be used with other machines. The interferometer scans independently from the other hardware, as indicated by the direction of the arrows in Fig. 5. The acquisition hardware is based on a personal computer (PC) (486DX2), a 16-bit ADC expansion card (DAS1800HR) from Keithley Metrabyte (Taunton, MA), and a generic counter-expansion card. The home-made digital electronics does the recording of the mirror speed, a number of pulse-shaping functions, and some error checking. This implementation is available commercially as a low-cost add-on and software package for use with any continuous-scan Fourier spectrometer.[11]

Figure 6 shows a block diagram of the speed-recording electronics. A quartz-stabilized time base of 28.332 MHz allows a timing accuracy of 35 ns. A 16-bit counter mea-
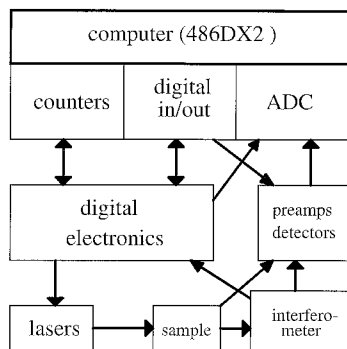
FIG. 5. Block diagram of the experimental setup. It shows the signal flow between the standard laser–sample–interferometer–detector combination and the control and acquisition electronics.

sures the time following a SYNC pulse, which has a known relation to the excitation of the sample. The counter overflows every 2.3 ms, allowing an unambiguous detection of mirror speeds as slow as 0.015 cm/s. Every time a HeNe reference pulse arrives, the counter value is stored in a static-memory chip, and the address used for storing is incremented. After the mirror speed is recorded for a sufficient amount of time, the data are read under software control using digital input and output. At a typical mirror speed of 0.3 cm/s, where alignment is stable and the speed variations are smallest (for our DA8), the time between HeNe reference pulses is 105 μs, which can be measured with a relative accuracy of 0.33×10^{-3}. For smoothly varying mirror speed, one can expect the results of the cubic spline interpolation, i.e., the path-length-difference values of the sample locations, to have an accuracy of 0.33×10^{-3} fringes. For comparison, the FTS6000 step-scan research-grade Fourier transform infrared (FT-IR) instruments from Bio-Rad specify a positional accuracy of 0.001 HeNe fringes and Bruker's instruments specify mirror stabilization to ≤1.5 nm (i.e., 0.005 HeNe fringes).

Two pieces of software have been implemented for the PC. The data-acquisition program synchronizes the transient initiation, interferogram and speed recording, and periodic error checking with the motion of the scanning mirror. The analysis program evaluates the speed information and finds the phase-corrected spectra (see Appen-
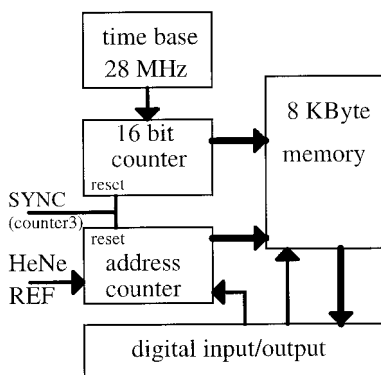
FIG. 6. Schematic diagram of speed-recording circuitry. The speed information is recorded as the time between HeNe reference pulses. The time base allows a resolution of 35 ns for a relative accuracy of typically 0.33×10^{-3} or better.
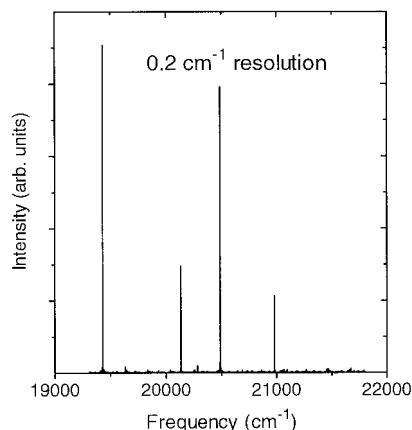
FIG. 7. Spectrum of a multiline Ar^{+} laser, set to medium power and chopped by an acoustooptical modulator, taken 10 μs after beam turn-on. It shows perfect frequency accuracy, good signal-to-noise ratio, and no artifacts.

dix). The latter program also runs on a UNIX workstation (Sun Microsystems, Inc.).

RESULTS AND DISCUSSION

A number of experiments were performed to test the performance of our implementation. First, a multiline Ar^{+}-laser beam was directed into the spectrometer by an acoustooptical (AO) modulator in 800-μs-long pulses as a test of gated data acquisition for an intermittent source. For attenuation, only the light scattered off a piece of paper was used and was further limited by a 1.5-mm aperture. A resolution of 0.2 cm^{-1} was chosen. Figure 7 shows the spectrum 10 μs after the modulator was turned on, with good signal-to-noise ratio and no artifacts related to the interleaved data acquisition. We observed four lines at the chosen laser power level. The center frequencies, estimated by a line-fitting technique, differ from those obtained with continuous-wave (CW) measurements using the same external setup and the DA8-acquisition tools by less than 0.1 cm^{-1} (half of the resolution). The uncertainty in relative peak heights (Table I), as determined by comparison with a 100-scan CW measurement, was only slightly more for a time-resolved than for a single-scan CW measurement. Transient pointing instabilities of the relatively slow AO modulator could be responsible. Another common problem in narrow-line emission measurements using Fourier spectroscopy is the occurrence of phase errors in regions without signal. Evidence for phase errors in both time-resolved and CW spectra is revealed in Fig. 8 by slight asymmetries and negative features near one of the lines. We chose to use only the standard phase correction to show the potential of our method and for consistency with the CW mea-

TABLE I. Relative strengths of Ar^{+}-laser lines measured in CW and time-resolved regimes.

Line	1-Scan TRFTS	1-Scan CW	100-Scan CW
1	1.14	0.90	0.98
2	0.37	0.41	0.44
3	1	0.93	1[a]
4	0.27	0.18	0.19

[a] This line was used for normalizing the third and fourth columns.
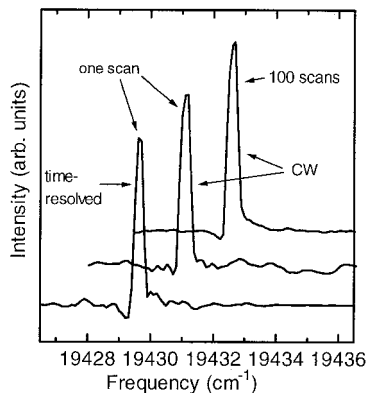
FIG. 8. A single Ar$^+$-laser line measured in time-resolved and CW mode. The slight asymmetries arise from imperfections in the phase characterization—a common problem with narrow-width emission sources. The time-resolved spectrum has about the same signal-to-noise ratio as the single-scan CW spectrum.

FIG. 9. Time-resolved $^4F_{3/2}$ to $^4I_{11/2}$ emission spectra (portion) for Nd: KLiYF$_5$ at 80 K. An energy transfer process is revealed with good signal-to-noise and no artifacts. The temporal spacing between the spectra is 11 μs.

surements. The multiline Ar$^+$-laser experiments (Figs. 7 and 8) using event-locked TRFTS with three samples per HeNe fringe at uneven intervals demonstrate a quality similar to the usual CW spectrum taken under identical conditions (except for the pulsing of the laser beam and four samples per fringe).

For a more realistic test with a natural transient phenomenon, we excited the laser crystal Nd:KLiYF$_5$ with a DCM-dye laser pumped by a Q-switched and doubled Nd:YAG laser. This crystal provides two crystallographic sites for the Nd^{3+} ions.[12] Ions in the different sites can be separately excited and have distinguishable photoluminescence spectra. Figure 9 shows a sequence of photoluminescence spectra at a sample temperature of 80 K with a resolution of 1 cm^{-1}. After short-pulse excitation at 15,991 cm^{-1} ($^2H_{11/2}$), the ions relax rapidly towards the $^4F_{3/2}$ manifold, from which the observed emission originates. All spectra were taken in a single experiment (one laser shot per interferogram point without coaddition) at time intervals of 11 μs, starting 8 μs after the excitation. Four distinguishable pairs of lines are shown. The left line in each pair belongs to the excited site and shows strong emission at early times. Energy is transferred nonradiatively to ions in the nonexcited site, resulting in an increase in their emission during the first 50 μs. At long times, the excited populations for the two sites approach an equilibrium, and the lines within each pair have approximately equal strength. The spectra show good signal-to-noise ratio, no phase errors, and no artifacts. This quality has been achieved in spite of 50% shot-to-shot variations in excitation energy through the use of a reference detector, which observes the sample's signal directly without the interferometer modulation (the direct arrow from the sample to the detectors in Fig. 5).

Another example with higher demands on the time resolution is the crystal (Yb, Ho):KYF$_4$, which has been recently studied as an IR-pumped upconversion laser at green wavelengths.[13] We studied various Ho to Yb back-transfer pathways.[14] Figure 10 shows the emission in the near-IR after excitation of a subgroup of the Ho dopant ions (class I) to the $^5F_5$ manifold. The spectra span the time interval from 1 to 43 μs (back to front) after excitation in 1-μs steps. Due to the limited sampling rate of
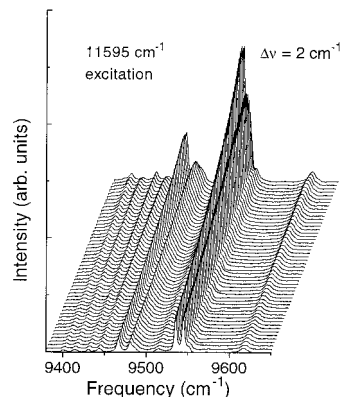
our current ADC (<98 kHz), the data acquisition was split into 11 groups, spreading the initial delay over the range from 1 to 11 μs. Degradation of the dye in the exciting laser and scattering on ice forming on the sample (80 K) during the course of the experiment may be responsible for a small reduction of total luminescence intensity, which is seen in Fig. 10 as the slight oscillation in the Yb peak intensity after collation of the various time delays into one plot. To demonstrate the unmodified performance of our system, we attempted no correction, although our analysis software could easily do so. Without averaging, the spectra have a signal-to-noise ratio adequate for the analysis of rise and decay times and the energy transfer rate. More (Ho, Yb):KYF$_4$ spectra measured with our setup are presented elsewhere.[14]

The following experiment shows that our implementation also works well in the far-infrared. P-doped Ge has been shown to emit far-IR radiation when exposed to crossed electric and magnetic fields.[15] The emission typically lasts only 300 ns, which is beyond our current time resolution. However, using a slow 4 K bolometer, we measured the time-integrated spectrum of this pulsed source. The spectrum obtained from a single scan with a resolution of 0.2 cm^{-1} is shown in Fig. 11. It shows several modes that can be explained in terms of multiple total internal reflections in the Ge crystal. The signal-to-noise ratio is quite good considering the high resolu-
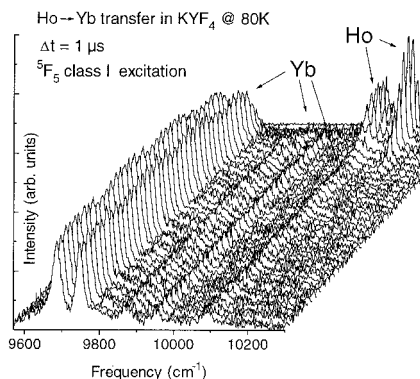
FIG. 10. Emission spectra at 80 K of Ho^{3+} and Yb^{3+} in KYF$_4$. The 1-μs steps show the rapid energy transfer from Ho^{3+} to Yb^{3+} ions.
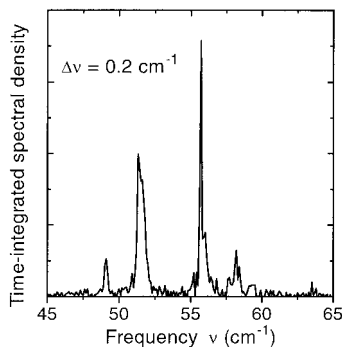
FIG. 11. Far-infrared emission from a pulsed p-Ge source at a resolution of 0.2 cm^{-1}.

FIG. 12. Mid-infrared emission from Er^{3+}:YLF at room temperature after long-pulse excitation with a 970-nm laser diode.

tion, no signal averaging, and the fact that no reference detector was used.

Figure 12 shows mid-IR emission of Er^{3+} in YLiF$_4$ at room temperature. The emission was excited by 4-ms-long pulses of a closely coupled 970-nm laser diode and detected after diode turnoff with an InSb detector at 77 K. The spectra with 4 cm^{-1} resolution have a temporal separation of 100 μs and cover a period of 4 ms. The signal-to-noise ratio obtained, though compromised by a large (>95%) black-body contribution to the total detector signal (partially from the hot semiconductor element near the sample), is sufficient to extract line positions and decay times.

CONCLUSION

Our new method of TRFTS eliminates the requirement of sampling the interferogram at evenly spaced path-length differences. Sampling instead at constant *time* intervals avoids artifacts arising from mirror-speed variations and makes the experiment more flexible. The sampling times can be chosen arbitrarily and are not tied to the available choice of mirror speeds. This capability also means that the mirror speed can be chosen to suit other demands. The ability to sample at more or less arbitrary pathlength differences has applications beyond inter-leaved data acquisition and may improve the performance of systems with one transient event per fringe (noninter-leaved). Decoupling the timing from the HeNe fringe pattern also allows measurement of events with random temporal spacing.

We have demonstrated the performance of our current implementation with a time resolution of 1 μs over a wide frequency range from far-infrared to visible at high resolution. The method itself does not impose restrictions on time scale, optical-frequency range, or spectral resolution. The addition of this technique to any continuous-scan interferometer enables time-resolved measurements over the entire frequency-resolution range this machine has for CW measurements. The signal-to-noise ratio obtained would depend on the particular transient event under investigation (as it does for step-scan interferometers). For a few selected cases, we have shown results with quality similar to CW measurements. Time resolution is currently limited by the sampling-time window of the ADC and the bandwidth of our preamplifier/detector combinations. The next goal is an improvement
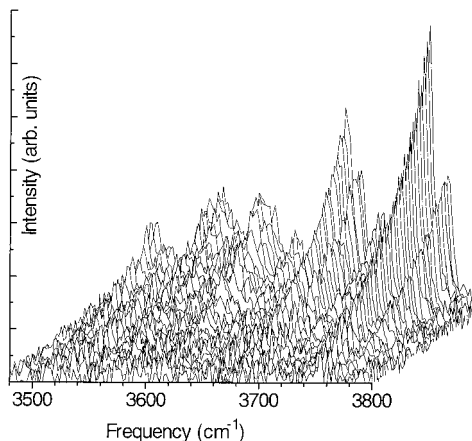
to about 10-ns resolution by using new high-speed 12-bit ADCs together with appropriate amplifiers and detectors.

1. J. J. Sloan and E. J. Kruus, in *Time Resolved Spectroscopy,* R. J. H. Clark and R. E. Hester, Eds. (Wiley, New York, 1989), Chap. 5, pp. 219–253.
2. T. Nakano, T. Yokoyama, and H. Toriumi, Appl. Spectrosc. **47,** 1354 (1993).
3. Bruker Instruments, Inc., product information October 1995.
4. H. Weidner and R. E. Peale, Appl. Opt. **16,** 2849 (1996).
5. J. Lindner, J. K. Lundberg, R. M. Williams, and S. R. Leone, Rev. Sci. Instrum. **66,** 2812 (1995).
6. J. T. McWhirter and A. J. Sievers, Appl. Spectrosc. **45,** 1391 (1991).
7. K. Masutani, H. Sugisawa, A. Yokota, Y. Furukawa, and M. Tasumi, Appl. Spectrosc. **46,** 560 (1992).
8. S. A. Rogers and S. R. Leone, Appl. Spectrosc. **47,** 1430 (1993).
9. S. A. Teukolsky, W. T. Vetterling, and B. P. Fannery, *Numerical Recipes in C: The Art of Scientific Computing,* W. H. Press, Ed. (Cambridge University Press, Cambridge, 1994), 3rd ed., Chap. 13, pp. 575–584.
10. D. Lafontaine, *Application Notes IMZ9641* (Bomem Inc., Québec, 1986).
11. Zaubertek, Inc., Oviedo, Florida 32765.
12. P. L. Summers, H. Weidner, R. E. Peale, and B. H. T. Chai, J. Appl. Phys. **75,** 2184 (1994).
13. R. J. Thrash, R. H. Jarman, B. H. T. Chai, and A. Pham, in *Compact Blue-Green Lasers,* 1994 Technical Digest Series (Optical Society of America, Washington, D.C., 1994), Vol. 1, pp. 73–75.
14. C. J. Schwindt, H. Weidner, J. Donahue, and R. E. Peale, "Time Resolved Fourier Spectroscopy of Energy Transfer in (Ho, Yb): KYF$_4$", in *OSA TOPS on Advanced Solid State Lasers,* S. A. Payne and C. Pollock, Eds. (Optical Society of America, Washington, D.C., 1996), pp. 534–538.
15. K. Park, R. E. Peale, H. Weidner, and J. J. Kim, J. Quant. Elect. **32,** 1203 (1996).

APPENDIX

The analysis of the unevenly spaced interferogram is split into two main steps: (1) finding the spectral density and (2) estimation and removal of unwanted phase information. Both steps rely on LS fits of harmonic functions to the interferogram data:

$$A \cos(2\pi\sigma x - \phi) \qquad (1)$$

where x is the pathlength difference and A and ϕ are functions of the optical frequency, σ. In application of the LS fitting, the goal is to minimize the sum:

$$S_{sq} = \sum [y_i - A \cos(2\pi\sigma x_i - \phi)]^2, \qquad (2)$$

which is to be taken over all N interferogram points (x_i, y_i) in the desired range of x values. With the use of the definitions

$$p \equiv A \cos \phi \qquad (3)$$

and

$$q \equiv A \sin \phi, \qquad (4)$$

subsequent calculations are simplified by putting Eq. 2 in the form

$$S_{sq} = \sum [y_i - p \cos 2\pi\sigma x_i - q \sin 2\pi\sigma x_i]^2. \qquad (5)$$

The minimum of S_{sq} with respect to the fitting parameters p and q is found by solving $\delta S_{sq}/\delta p = 0$ and $\delta S_{sq}/\delta q = 0$ simultaneously. With the definitions

$$Y_C \equiv \sum y_i \cos(2\pi\sigma x_i), \qquad (6)$$

$$Y_S \equiv \sum y_i \sin(2\pi\sigma x_i), \qquad (7)$$

$$C_2 \equiv \sum \cos(2\pi\sigma 2 x_i), \qquad (8)$$

and

$$S_2 \equiv \sum \sin(2\pi\sigma 2 x_i) \qquad (9)$$

one obtains

$$p = 2(Y_C(N - C_2) - Y_S S_2)/(N^2 - C_2^2 - S_2^2) \qquad (10)$$

$$q = 2(Y_S(N + C_2) - Y_C S_2)/(N^2 - C_2^2 - S_2^2). \qquad (11)$$

From Eqs. 3, 4, 10 and 11, we can find the phase ϕ as

$$\phi(\sigma) = \arctan(q/p), \qquad (p \geq 0)$$

or

$$\phi(\sigma) = \arctan(q/p) + \pi, \qquad (p < 0). \qquad (12)$$

Using all measured interferogram points in the range $[-x_z, X_z]$ with $X_z > x_z$ and treating ϕ now as a known constant at each value σ, $\delta S_{sq}/\delta A = 0$ yields

$$A(\sigma) = 2(Y_C \cos \phi + Y_S \sin \phi)$$
$$\div (N + C_2 \cos 2\phi + S_2 \sin 2\phi), \qquad (13)$$

which represents the phase-corrected spectral density at frequency σ. Evaluating A for the frequencies of interest gives the phase-corrected spectrum.

In the limit of equal spacing of interferogram points (Δx) and spectrum points ($\Delta\sigma = 1/(N \Delta x)$), we find $C_2 \rightarrow 0$ (Eq. 8) and $S_2 \rightarrow 0$ (Eq. 9). This reduces p and q (Eqs. 10 and 11) to the real and imaginary parts of a complex

FFT, respectively. In the same limit, the expression for A becomes the real part of the product of an FFT with $e^{-i\phi}$, which is also the result of the Mertz method[10] of obtaining phase-corrected spectra.

The evaluation of Eqs. 6–9 can be done in a number of ways. The resemblance to the equations of the discrete Fourier transform is only superficial since the summation is over irregularly spaced data points. The straightforward calculation of a spectrum with N points requires on the order of $N \times N$ calls to trigonometric functions, which is very time consuming. The uneven spacing of interferogram points prohibits the use of efficient recurrence relations. The following technique[9] can be more than 100 times faster for practical interferogram sizes. The evaluation of Eqs. 6–9 with full machine accuracy is replaced by an approximation using Lagrange interpolation; i.e., the value of a trigonometric function $g(x_i)$ (the sines and cosines in Eqs. 6–9) at an arbitrary pathlength difference x_i is approximated from values of this function at nearby points $\{x_k'\}$ on a regular grid according to

$$g(x_i) = \sum w_k(x_i) g(x_k') \qquad (14)$$

with the Lagrange coefficients

$$w_k(x_i) = \prod_{l \neq k}(x_i - x_l') \Big/ \prod_{l \neq k}(x_k' - x_l'). \qquad (15)$$

Equations 6–9 can now be approximated as

$$\sum y_i g(x_i) \approx \sum y_i \left[\sum w_k(x_i) g(x_k') \right]$$
$$= \sum \left[\sum y_i w_k(x_i) \right] g(x_k')$$
$$= \sum y_k' g(x_k'), \qquad (16)$$

with

$$y_k' = \sum y_i w_k(x_i). \qquad (17)$$

For Eqs. 8 and 9, one uses $y_i \equiv 1$. Hence, the sum over the irregular interferogram on the left side has been replaced by a sum over a regular mesh (right side). The latter is now suitable for evaluation using FFT, which requires only on the order of $N \log_2 N$ operations. The original interferogram points are "spread" over the regular mesh by finding the y_k' before the sine and cosine transforms, which can then be evaluated simultaneously by using a complex FFT. Now the relationship between the LS fitting result (Eq. 13) and the usual FFT method is even more obvious. The numerator in Eq. 13 is the phase-corrected result of a complex FFT from a regular-mesh approximation of the measured interferogram. The denominator is a correction factor that depends only on the actual distribution of the samples.